

# CrossFusion: A Multi-Scale Cross-Attention Convolutional Fusion Model for Cancer Survival Prediction

Rustin Soraki<sup>1</sup>, Huayu Wang<sup>1</sup>, Joann G. Elmore<sup>2</sup>, and Linda Shapiro<sup>1</sup>

<sup>1</sup> University of Washington, Seattle, WA 98195, USA

<sup>2</sup> David Geffen School of Medicine, UCLA, Los Angeles, CA 90024, USA  
rustin@cs.washington.edu

**Abstract.** Cancer survival prediction from whole slide images (WSIs) is a challenging task in computational pathology due to the large size, irregular shape, and high granularity of the WSIs. These characteristics make it difficult to capture the full spectrum of patterns, from subtle cellular abnormalities to complex tissue interactions, which are crucial for accurate prognosis. To address this, we propose CrossFusion—a novel, multi-scale feature integration framework that extracts and fuses information from patches across different magnification levels. By effectively modeling both scale-specific patterns and their interactions, CrossFusion generates a rich feature set that enhances survival prediction accuracy. We validate our approach across six cancer types from public datasets, demonstrating significant improvements over existing state-of-the-art methods. Moreover, when coupled with domain-specific feature extraction backbones, our method shows further gains in prognostic performance compared to general-purpose backbones. The source code is available at: <https://github.com/RustinS/CrossFusion>

**Keywords:** Computer Vision · Computational Pathology · Survival Prediction · Cross-Attention · Multi-Scale Image Processing.

## 1 Introduction

Whole Slide Images (WSIs) capture critical tumor characteristics and are central to modern cancer diagnosis [10,9,5]. In clinical practice, survival analysis based on WSIs plays a vital role in informing prognosis and guiding treatment strategies [1]. Recent advances in survival analysis have leveraged multiple-instance learning (MIL) and deep learning. For instance, Ilse et al. [8] employ attention mechanisms to identify the most predictive regions, while Li et al. [11] aggregate instance-level features into robust slide-level representations. Transformer-based approaches [15] capture long-range dependencies and graph-based methods [12,3] model spatial relationships effectively. More recently, methods by Yang et al. [19] and Wu et al. [16] have enhanced interpretability and prediction by integrating sparse attention and prototypical representations. Despite these advancements, the enormous size and heterogeneity of WSIs make it challenging for AI models

to capture high-level global tissue patterns and fine-grained cellular detail, both essential for robust survival analysis.

A multi-scale approach offers a promising solution by combining large patches that provide an overview of tissue architecture with small patches that capture detailed cellular morphology. By merging coarse structural cues with fine-grained details, multi-scale methods can better reflect the complex biological processes underlying tumor development and progression. Prior studies have shown that integrating information across multiple scales significantly improves diagnostic accuracy and reduces errors. For example, Deng et al. [4] employ cross-scale attention maps to aggregate features, while Wu et al. [17] use features from different scales as keys, queries, and values to guide learning. Similarly, Zhao et al. [20] select informative patches using a variational positive-unlabeled framework and fuse them with cross-attention. However, these approaches often overlook certain resolution levels or rely on suboptimal fusion techniques, leaving two key challenges unresolved: effectively combining complementary information from multiple scales and developing robust methods for fusing these features.

To address these challenges, we propose **CrossFusion**, a novel framework that unifies multi-scale patch embeddings from WSIs into a single, predictive representation. We summarize our main contributions as follows:

1. **Multi-Scale Cross-Attention:** This module enables interaction between features at different resolutions, allowing high-resolution details and low-resolution global patterns to reinforce each other while preserving spatial context.
2. **Convolution-Based Fusion:** By balancing local and global cues, this fusion strategy reduces redundancy and enhances the discriminative power of the combined features.
3. **Extensive Validation:** We validate CrossFusion on diverse cancer survival datasets, demonstrating that it matches or exceeds state-of-the-art performance in survival analysis while maintaining interpretability through visualization of key regions at multiple magnifications. We also examine the effect of different feature extraction backbones and compare CrossFusion trained on the domain-specific backbones to the general one.

## 2 Method

This section outlines the pipeline of our proposed methodology, CrossFusion. Figure 1 illustrates the complete framework, including its main stages and components. As shown in the figure, the extracted patches at different magnifications are encoded by a feature extractor, projected into a common embedding space, and then through the Cross-Attention Block, in which the different magnifications interact. The next step is the Pad-Transformer process, which uses Pyramid Position Encoding to capture local and global context. The Conv Processor is used to fuse the multi-scale features.

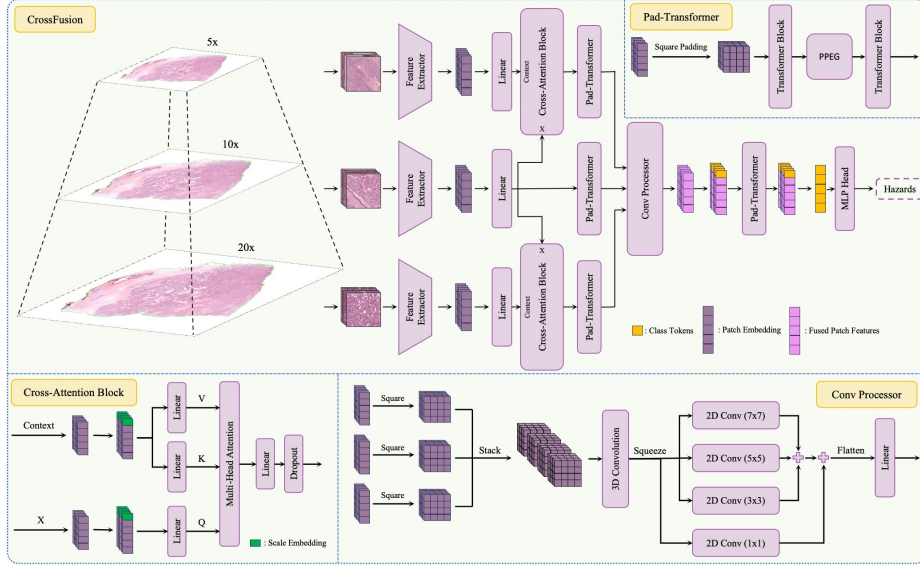


Fig. 1: Overview of CrossFusion. WSIs are processed by extracting patches at 5x (coarse), 10x (source), and 20x (fine) magnifications, which are first encoded using a feature extractor and then projected into a common embedding space. The source features interact with the coarse and fine features via cross-attention blocks, and each branch is refined by Pad-Transformers. The multi-scale features are subsequently fused using a Conv Processor, and a replicated learnable class token is appended. An additional transformer block refines this token, and an MLP head produces the final survival predictions from the class tokens.

## 2.1 CrossFusion

The CrossFusion module takes three inputs:  $\mathbf{X}_C$  (coarse),  $\mathbf{X}_S$  (source), and  $\mathbf{X}_F$  (fine), which represent patch embeddings from 5x, 10x, and 20x magnifications, respectively. Initially, each embedding is projected into a shared space  $D_e$ . Next, to facilitate inter-scale interactions, the module applies cross-attention with  $\mathbf{X}_S$  as the query and the other embeddings as context:

$$\mathbf{X}'_C = CAB(\mathbf{X}_S, \mathbf{X}_C), \quad \mathbf{X}'_F = CAB(\mathbf{X}_S, \mathbf{X}_F) \quad (1)$$

where  $CAB$  denotes the Cross-Attention Block. Each feature set is then processed by dedicated Pad-Transformer ( $PT$ ) blocks. The outputs are fused via the Conv Processor ( $CP$ ):

$$\mathbf{X}_{\text{fused}} = CP\left(PT(\mathbf{X}'_C), PT(\mathbf{X}_S), PT(\mathbf{X}'_F)\right) \quad (2)$$

A learnable class token  $\mathbf{c} \in \mathbb{R}^{1 \times D_e}$  is first replicated and prepended to the fused token sequence. This extended sequence is processed by an additional Pad-Transformer followed by Layer Normalization. The class token is then extracted

to yield  $\mathbf{c}'$ . An MLP head maps  $\mathbf{c}'$  to logits  $\mathbf{l}$ , from which hazards  $\mathbf{h}$  are computed using a sigmoid activation. Finally, survival probabilities  $\mathbf{S}$  are obtained as the cumulative product of  $1 - \mathbf{h}$ .

## 2.2 Cross-Attention Block

The cross-attention module fuses information from two inputs: the primary input  $\mathbf{X} \in \mathbb{R}^{B \times N \times D}$  and a contextual input **Context**  $\in \mathbb{R}^{B \times M \times D}$ , where  $B$  is the batch size,  $N$  and  $M$  are sequence lengths, and  $D$  is the embedding dimension. Both inputs are augmented with a learnable scale embedding  $\mathbf{s} \in \mathbb{R}^{1 \times 1 \times D}$  before computing attention, acting like a learnable positional encoding. The queries, keys, and values are obtained via linear projections:

$$\mathbf{Q} = W_q(\mathbf{X} + \mathbf{s}), \quad \mathbf{K} = W_k(\mathbf{Context} + \mathbf{s}), \quad \mathbf{V} = W_v(\mathbf{Context} + \mathbf{s}), \quad (3)$$

where  $W_q, W_k, W_v \in \mathbb{R}^{D \times D}$  are learnable weight matrices. Multi-head attention is then applied, followed by an output projection. The output is further processed through residual connections, layer normalization, and a feed-forward network. This mechanism enables effective information exchange between the primary input and its contextual counterpart, improving feature representation.

## 2.3 Pad-Transformer

The Pad-Transformer organizes input tokens into a grid, processes them with an initial Transformer block, uses Pyramid Position Encoding Generator (PPEG) [15] to add spatial context, and then further refines the features using a second Transformer block. This combines global dependencies (from the first block) and local details (via PPEG) before final refinement by the second Transformer block.

**Square Padding** Given an input sequence  $\mathbf{X} \in \mathbb{R}^{B \times N \times D}$ , where  $N$  is the number of tokens, we first compute  $H = W = \lceil \sqrt{N} \rceil$ . We then pad  $\mathbf{X}$  by appending the first  $(H \times W) - N$  tokens to the end of the sequence, resulting in a sequence of length  $H \times W$ . Finally, this padded sequence is reshaped into a square grid  $\mathbf{X}_s \in \mathbb{R}^{B \times H \times W \times D}$  for subsequent spatial operations.

**Transformer Blocks** Each transformer block applies layer normalization, computes multi-head self-attention, and adds the result to the input via a residual connection. A second layer normalization is followed by a feed-forward network, GELU activation, and dropout.

**Convolutional Positional Encoding (PPEG)** To incorporate local spatial context, the PPEG module applies three parallel depth-wise convolutions with kernel sizes 7, 5, and 3 to the reshaped feature map  $\mathbf{X}_s \in \mathbb{R}^{B \times D \times H \times W}$ :

$$\mathbf{X}_{\text{PPEG}} = \text{Conv}_7(\mathbf{X}_s) + \text{Conv}_5(\mathbf{X}_s) + \text{Conv}_3(\mathbf{X}_s) + \mathbf{X}_s \quad (4)$$

This operation enhances token representations with detailed local positional information.

## 2.4 Conv Processor

The Conv Processor fuses multi-source features and enhances spatial representations using multi-scale convolutions. Given three input sequences  $\mathbf{X}_i \in \mathbb{R}^{B \times N \times D}$ ,  $i \in \{1, 2, 3\}$ , each is square-padded and reshaped into a 2D feature map,  $\mathbf{X}'_i \in \mathbb{R}^{B \times D \times H \times W}$ , where  $N = H \times W$ . The feature maps are stacked into  $\mathbf{X}_{\text{stack}} \in \mathbb{R}^{B \times 3 \times D \times H \times W}$  and fused via a 3D convolution to get  $\mathbf{X}_{\text{fused}}$ . After squeezing the singleton channel, multi-scale features are extracted by applying parallel depth-wise convolutions with kernel sizes 7, 5, 3, and 1, where the output dimension is reduced to  $D' = D//2$ :

$$\mathbf{X}_{\text{ms}} = \text{Conv}_7(\mathbf{X}_{\text{fused}}) + \text{Conv}_5(\mathbf{X}_{\text{fused}}) + \text{Conv}_3(\mathbf{X}_{\text{fused}}) + \text{Conv}_1(\mathbf{X}_{\text{fused}}). \quad (5)$$

The resulting feature map is flattened along spatial dimensions into  $\mathbf{X}_{\text{flat}} \in \mathbb{R}^{B \times D' \times (H \cdot W)}$  and permuted into a token sequence  $\mathbf{X}_{\text{seq}} \in \mathbb{R}^{B \times (H \cdot W) \times D'}$ . Finally, a linear projection followed by Layer Normalization restores the original dimension ( $D$ ). This module efficiently fuses multi-source information while capturing multi-scale spatial features.

## 3 Experimental Setup

### 3.1 Dataset

We used H&E WSIs from six TCGA cancer types: BLCA (437 slides), BRCA (1016 slides), COAD (424 slides), GB&LGG (1041 slides), LUAD (507 slides), and UCEC (539 slides). These datasets were chosen for their size, public availability, survival follow-up data, and a balanced uncensored-to-censored ratio (average 0.28). On average, each WSI yields 13,496 patches at 20x, 3,449 patches at 10x, and 895 patches at 5x, with the number of 20x patches reaching up to 137,990.

### 3.2 Implementation Details

*Patch Extraction and Embedding:* We used CLAM [14] to extract  $256 \times 256$  patches at 20x, 10x, and 5x magnifications and extract features from different feature extraction backbones. Tissue regions were identified using a binary mask computed by thresholding the saturation channel in HSV.

Table 1: C-Index (mean<sub>std</sub>) of different methods over the six different datasets. The best and the second-best results are highlighted in **bold** and underline, respectively.

	BLCA	BRCA	COAD	GB&LGG	LUAD	UCEC
AMIL	.559 <sub>.059</sub>	.590 <sub>.050</sub>	.662 <sub>.063</sub>	.759 <sub>.111</sub>	.590 <sub>.036</sub>	.644 <sub>.092</sub>
DSMIL	.552 <sub>.050</sub>	.564 <sub>.044</sub>	.610 <sub>.012</sub>	.728 <sub>.102</sub>	.579 <sub>.032</sub>	.601 <sub>.073</sub>
TransMIL	.574 <sub>.064</sub>	.594 <sub>.045</sub>	.656 <sub>.057</sub>	.772 <sub>.093</sub>	.594 <sub>.059</sub>	.664 <sub>.044</sub>
DeepGraphSurv	.572 <sub>.054</sub>	.558 <sub>.099</sub>	.591 <sub>.119</sub>	.764 <sub>.053</sub>	.622 <sub>.055</sub>	.635 <sub>.061</sub>
PatchGCN	.563 <sub>.043</sub>	.595 <sub>.089</sub>	.612 <sub>.144</sub>	.774 <sub>.046</sub>	.577 <sub>.081</sub>	.679 <sub>.071</sub>
SCMIL	.566 <sub>.054</sub>	.590 <sub>.034</sub>	<u>.677<sub>.070</sub></u>	.763 <sub>.094</sub>	.584 <sub>.050</sub>	.668 <sub>.071</sub>
ProtoSurv	.579 <sub>.023</sub>	.627 <sub>.034</sub>	.668 <sub>.057</sub>	.776 <sub>.031</sub>	.619 <sub>.046</sub>	<b>.730<sub>032</sub></b>
CrossFusion w/o CP	<u>.627<sub>.014</sub></u>	<u>.631<sub>.076</sub></u>	.669 <sub>.069</sub>	<u>.787<sub>.081</sub></u>	<u>.627<sub>.038</sub></u>	<u>.710<sub>.061</sub></u>
CrossFusion w/o F&C	.562 <sub>.058</sub>	.629 <sub>.052</sub>	.631 <sub>.052</sub>	.782 <sub>.074</sub>	.609 <sub>.053</sub>	.672 <sub>.050</sub>
<b>CrossFusion</b>	<b>.630<sub>.027</sub></b>	<b>.643<sub>.037</sub></b>	<b>.694<sub>.053</sub></b>	<b>.797<sub>.056</sub></b>	<b>.627<sub>.040</sub></b>	.702 <sub>.044</sub>

*Training and Evaluation:* The model was trained with Adam (learning rate  $1 \times 10^{-4}$ , weight decay  $4 \times 10^{-6}$ , batch size 1) with a 5-epoch warm-up, and evaluated via 5-fold cross-validation. For a fair comparison, all methods used the same loss function, feature embeddings, and hyperparameters. Experiments were implemented in PyTorch on a workstation with four Nvidia RTX A4000 GPUs.

*Evaluation Metrics:* Performance was measured using the mean C-index across validation splits. For qualitative assessment, Kaplan-Meier curves are used to visualize patient stratification, distinguishing low- and high-risk groups based on survival distributions.

## 4 Experiments and Results

In this section, we evaluate our model’s performance through experiments. First, we compare CrossFusion to state-of-the-art methods. Next, we assess our model’s interpretability by analyzing attention-based heatmaps, providing insights into its decision-making process. Finally, we analyze the effect of using different foundational models as feature extraction backbones to determine whether domain-specialized backbones improve performance.

### 4.1 Comparison with State-Of-The-Art Methods

We evaluated CrossFusion against state-of-the-art survival prediction methods: AMIL [8], DSMIL [11], TransMIL [15], DeepGraphSurv [12], Patch-GCN [3], SCMIL [19], and ProtoSurv [16]. All models used ResNet50 [6] as the feature extractor for fair comparison.

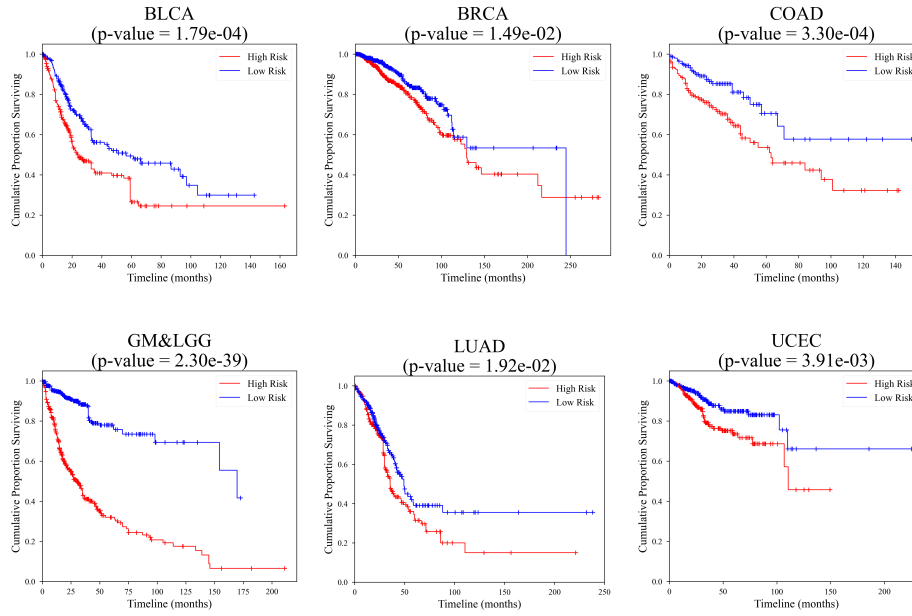


Fig. 2: Kaplan-Meier curves of predicted high-risk (red) and low-risk (blue) groups. A P-value  $< 0.05$  indicates statistical significance.

As shown in Table 1, CrossFusion achieves the best or near-optimal performance across six cancer datasets. In the UCEC dataset, the low uncensored-to-all-slides ratio (0.15) posed a challenge due to CrossFusion’s reliance on patch-level features without prior information, resulting in slightly lower performance than ProtoSurv, which leverages priors. Nevertheless, CrossFusion consistently outperforms all other baselines and remains competitive with ProtoSurv, demonstrating robustness even under data constraints.

Ablation studies validated the contributions of key components. First, replacing the ConvProcessor (CP) with simple concatenation and linear projection of the three sources reduced performance across all datasets except UCEC, where scarce uncensored data posed a challenge for effectively training the convolutional layers of the ConvProcessor. Second, removing the Fine (F) and Coarse (C) sources and using  $20\times$  patches as the Source features significantly degraded performance in most datasets, confirming the necessity of multi-scale inputs for capturing discriminative WSI features.

Finally, we generated Kaplan-Meier plots and computed p-values to assess CrossFusion’s ability to stratify patients into high- and low-risk groups. As shown in Figure 2, the results highlight the model’s capability to effectively distinguish between these subgroups.

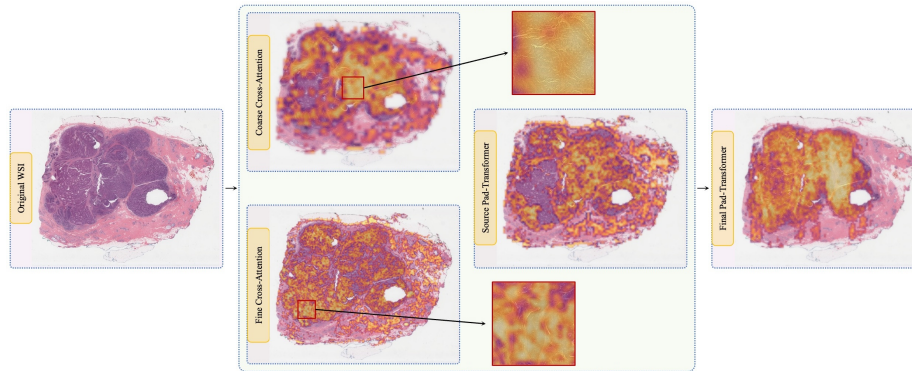


Fig. 3: Generated heatmaps from the model predicting a high-risk case. The dark purple clusters mark tumor regions in the original WSI on the left and lighter yellow areas highlight important regions from the model’s attention weights.

## 4.2 Interpretability

To explore the model’s decision-making, we generated heatmaps from attention weights in the Cross-Attention layers, the source features Pad-Transformer, and the fused features Pad-Transformer. Figure 3 shows a WSI from the TCGA-BRCA dataset—depicting a high-risk patient with low survival time—alongside its corresponding heatmaps.

The three intermediate heatmaps reveal that different modules capture distinct features: the Coarse Cross-Attention layer focuses on large-scale tissue organization, the Fine Cross-Attention layer captures detailed cellular morphology, and the Source Pad-Transformer emphasizes intermediate-scale structures. The final heatmap from the last transformer layer demonstrates that the model effectively filters out less relevant regions, concentrating on key histopathological features.

## 4.3 Analyzing the effect of Different Feature Extraction Backbones

We evaluate CrossFusion using different feature extraction backbones, comparing their impact on model performance. Specifically, we extract patch-level features using Conch [13], Uni2-h [2], QuiltNet [7], and Prov-GigaPath [18], and compare them against features extracted using ResNet50.

Table 2 shows that CrossFusion performs best with features from the Uni2-h backbone, while other domain-specific backbones yield similar results. The performance gap is highlighted particularly in the BRCA and the UCEC datasets, where utilizing high-quality features is crucial because of the low uncensored-to-all-slides ratio. The clear performance gap between CrossFusion trained on specialized backbones and CrossFusion trained on ResNet50 backbone highlights the benefit of domain-specific extraction backbones, which better capture tissue-level

Table 2: C-Index (mean<sub>std</sub>) of **CrossFusion** trained on different feature extraction backbones over the six different datasets. The best and the second-best results are highlighted in **bold** and underline, respectively.

	BLCA	BRCA	COAD	GB&LGG	LUAD	UCEC	Mean
w/ResNet50 (Base)	.630 <sub>.027</sub>	.643 <sub>.037</sub>	.694 <sub>.053</sub>	.797 <sub>.056</sub>	<u>.627<sub>.040</sub></u>	.702 <sub>.044</sub>	.682
w/Conch	<b>.649.053</b>	.675 <sub>.060</sub>	.705 <sub>.024</sub>	.799 <sub>.055</sub>	.604 <sub>.055</sub>	<u>.737<sub>.043</sub></u>	.695
w/Uni2-h	.628 <sub>.019</sub>	<u>.684<sub>.043</sub></u>	.698 <sub>.023</sub>	<u>.810<sub>.067</sub></u>	.625 <sub>.051</sub>	<b>.745.030</b>	<b>.698</b>
w/QuiltNet	.614 <sub>.050</sub>	.650 <sub>.017</sub>	<u>.712<sub>.043</sub></u>	<b>.812.032</b>	<b>.640.064</b>	.727 <sub>.028</sub>	.693
w/Prov-GigaPath	<u>.635<sub>.023</sub></u>	<b>.686.037</b>	<b>.718.064</b>	.802 <sub>.051</sub>	.620 <sub>.063</sub>	.724 <sub>.043</sub>	<u>.698</u>

details, such as cellular morphology and tissue architecture, crucial for accurate prognostication.

## 5 Conclusion

We introduced CrossFusion, a novel framework that fuses multi-scale patch embeddings from WSIs using cross-attention, transformer-based spatial encoding, and convolutional fusion. By integrating multi-scale features, CrossFusion captures key histopathological patterns linked to patient survival. Our experiments on diverse TCGA cancer datasets show that CrossFusion demonstrates significant improvements over the current state-of-the-art survival prediction methods, even under challenging conditions.

Our results underscore the value of domain-specific feature extraction in preserving crucial tissue details, such as cellular morphology and tissue architecture. The attention-based heatmaps further confirm the model’s effectiveness and offer insights into its decision-making process.

In summary, CrossFusion bridges advanced deep learning with clinical needs, providing a robust and interpretable tool for cancer survival prediction. Future work will explore additional data modalities to guide the model to focus on important case-specific patterns and enhance interpretability, paving the way for more personalized cancer treatment and improved patient outcomes.

## References

1. Campanella, G., Hanna, M.G., Geneslaw, L., Miralflor, A., Silva, V.W.K., Busam, K.J., Brogi, E., Reuter, V.E., Fuchs, T.J., Klimstra, D.S.: Clinical-grade computational pathology using weakly supervised deep learning on whole slide images. *Nature Medicine* **25**(8), 1301–1309 (2019)
2. Chen, R.J., Ding, T., Lu, M.Y., Williamson, D.F.K., Jaume, G., Chen, B., Zhang, A., Shao, D., Song, A.H., Shaban, M., et al.: Towards a general-purpose foundation model for computational pathology. *Nature Medicine* (2024)

3. Chen, R.J., Lu, M.Y., Shaban, M., Chen, C., Chen, T.Y., Williamson, D.F.K., Mahmood, F.: Whole slide images are 2d point clouds: Context-aware survival prediction using patch-based graph convolutional networks. In: *Medical Image Computing and Computer Assisted Intervention – MICCAI 2021*, pp. 339–349. Springer International Publishing (2021). [https://doi.org/10.1007/978-3-030-87237-3\\_33](https://doi.org/10.1007/978-3-030-87237-3_33)
4. Deng, R., Cui, C., Remedios, L.W., Bao, S., Womick, R.M., Chiron, S., Li, J., Roland, J.T., Lau, K.S., Liu, Q., et al.: Cross-scale multi-instance learning for pathological image diagnosis. *Medical image analysis* **94**, 103124 (2024)
5. Ghaznavi, F., Evans, A., Madabhushi, A., Feldman, M.: Digital imaging in pathology: whole-slide imaging and beyond. *Annual Review of Pathology: Mechanisms of Disease* **8**(1), 331–359 (2013)
6. He, K., Zhang, X., Ren, S., Sun, J.: Deep residual learning for image recognition. In: *Proceedings of the IEEE Conference on Computer Vision and Pattern Recognition (CVPR)* (June 2016)
7. Ikezogwo, W.O., Seyfioglu, M.S., Ghezloo, F., Chan Geva, D.S., Sheikh Mohammed, F., Anand, P.K., Krishna, R., Shapiro, L.: Quilt-1m: One million image-text pairs for histopathology. arXiv preprint arXiv:2306.11207 (2023)
8. Ilse, M., Tomczak, J.M., Welling, M.: Attention-based deep multiple instance learning. arXiv preprint arXiv:1802.04712 (2018)
9. Kothari, S., Phan, J.H., Stokes, T.H., Wang, M.D.: Pathology imaging informatics for quantitative analysis of whole-slide images. *Journal of the American Medical Informatics Association* **20**(6), 1099–1108 (2013)
10. Kumar, N., Gupta, R., Gupta, S.: Whole slide imaging (wsi) in pathology: current perspectives and future directions. *Journal of digital imaging* **33**(4), 1034–1040 (2020)
11. Li, B., Li, Y., Eliceiri, K.W.: Dual-stream multiple instance learning network for whole slide image classification with self-supervised contrastive learning (2021), arXiv preprint arXiv:2011.08939
12. Li, R., Yao, J., Zhu, X., Li, Y., Huang, J.: Graph cnn for survival analysis on whole slide pathological images. In: Frangi, A.F., Schnabel, J.A., Davatzikos, C., Alberola-López, C., Fichtinger, G. (eds.) *Medical Image Computing and Computer Assisted Intervention – MICCAI 2018*. pp. 174–182. Springer International Publishing, Cham (2018)
13. Lu, M.Y., Chen, B., Williamson, D.F.K., Chen, R.J., Liang, I., Ding, T., Jaume, G., Odintsov, I., Le, L.P., Gerber, G., et al.: A visual-language foundation model for computational pathology. *Nature Medicine* **30**, 863–874 (2024)
14. Lu, M.Y., Williamson, D.F.K., Chen, T.Y., Chen, R.J., Barbieri, M., Mahmood, F.: Data-efficient and weakly supervised computational pathology on whole-slide images. *Nature Biomedical Engineering* **5**(6), 555–570 (2021)
15. Shao, Z., Bian, H., Chen, Y., Wang, Y., Zhang, J., Ji, X., et al.: Transmil: Transformer based correlated multiple instance learning for whole slide image classification. *Advances in Neural Information Processing Systems* **34**, 2136–2147 (2021)
16. Wu, J., Ke, X., Jiang, X., Wu, H., Kong, Y., Shao, L.: Leveraging tumor heterogeneity: Heterogeneous graph representation learning for cancer survival prediction in whole slide images. In: *The Thirty-eighth Annual Conference on Neural Information Processing Systems* (2024)
17. Wu, W., Mehta, S., Nofallah, S., Knezevich, S., May, C.J., Chang, O.H., Elmore, J.G., Shapiro, L.G.: Scale-aware transformers for diagnosing melanocytic lesions. *IEEE Access* **9**, 163526–163541 (2021)

18. Xu, H., Usuyama, N., Bagga, J., Zhang, S., Rao, R., Naumann, T., Wong, C., Gero, Z., González, J., Gu, Y., Xu, Y., Wei, M., Wang, W., Ma, S., Wei, F., Yang, J., Li, C., Gao, J., Rosemon, J., Bower, T., Lee, S., Weerasinghe, R.: A whole-slide foundation model for digital pathology from real-world data. *Nature* (2024)
19. Yang, Z., Liu, H., Wang, X.: Scmil: Sparse context-aware multiple instance learning for predicting cancer survival probability distribution in whole slide images (2024), arXiv preprint arXiv:2407.00664
20. Zhao, B., Deng, W., Li, Z.H.H., Zhou, C., Gao, Z., Wang, G., Li, X.: Less: Label-efficient multi-scale learning for cytological whole slide image screening. *Medical Image Analysis* **94**, 103109 (2024)